EARTH SCIENCES
RESEARCH JOURNAL
Earth Sci. Res. J. Vol. 29, No. 2 (June, 2025): 219 - 230

UNIVERSIDAD NACIONAL DE COLOMBIA

GEOPHYSICS

Accuracy Assessment of the PPP Solution Using Standard GNSS Receivers

Vu Ngoc Quang[1], Luong Ngoc Dung[2,*], Nguyen Viet Ha[3], Tran Dinh Trong[2]
1 Department of Planning and Urban Transport, University of Transport Technology, Hanoi, Vietnam;
2 Department of Geodesy and Geomatics Engineering, Hanoi University of Civil Engineering, Hanoi, Vietnam;
3 Department of Engineering Surveying, Hanoi University of Mining and Geology, Hanoi, Vietnam;
*Corresponding author: dungln@huce.edu.vn
https://orcid.org/0000-0002-9957-5757 - LUONG Ngoc Dung
https://orcid.org/0000-0001-8960-772X - VU Ngoc Quang
https://orcid.org/0000-0002-3838-9950 - TRAN Dinh Trong
https://orcid.org/0000-0001-6246-8475 - NGUYEN Viet Ha

ABSTRACT

The introduction of the free PPP solution by the BDS-3 system and its published applications offers a feasible opportunity to conduct surveying tasks without the need to establish base stations. This paper examines the accuracy of the free PPP solution using a standard receiver integrated with this functionality to verify the technical specifications published in its documentation. The study utilises a ComNav N3 receiver to collect coordinate data from the PPP and near-baseline single-base RTK solutions for accuracy assessment. The results indicate that parameters such as the time to achieve a fixed solution and the reported accuracy align closely with the technical specifications. Additionally, the determination of relative distances and height differences between points in the designed experiment shows equivalence between the PPP solution and the RTK solution.

Keywords: GNSS-RTK, PPP solution, N3 GNSS, convergence, PPP accuracy

Evaluación de la precisión de la solución PPP utilizando receptores GNSS estándar

RESUMEN

El lanzamiento de una solución gratuita de posicionamiento preciso punto a punto (PPP) por el sistema BDS-3 y sus aplicaciones presentan una oportunidad factible de realizar tareas de sondeo sin la necesidad de establecer estaciones base. Este artículo examina la precisión de la solución PPP a través de un receptor estandar integrado con la funcionalidad de verificar las especificaciones técnicas publicadas en su documentación. Durante el estudio se utilizó un receptor ComNav N3 para recolectar datos de coordenadas del PPP y soluciones de base RTK para comparar la precisión. Los resultados indican que parámetros como el tiempo de adquisicion de respuesta y la precisión reportada se alinean con las especificaciones técnicas. Adicionalmente, la determinación de distancias relativas y el peso de las diferencias entre puntos en el experimento diseñado muestran una equivalencia entre la solución PPP y la solución RTK.

Palabras clave: Estaciones GNSS-RTK, solución de posicionamiento preciso punto a punto; receptor N3; convergencia; precisión.

Record
Manuscript received: 20/01/2025
Accepted for publication: 16/04/2025

How to cite this item:
Quang, V. N., Dung, L. N., Ha, N. V., Trong, T. D. (2025). Accuracy Assessment of the PPP Solution Using Standard GNSS Receivers. *Earth Sciences Research Journal, 29*(2), 219-230. https://doi.org/10.15446/esrj.v29n2.118407

1. Introduction

Dynamic Global Navigation Satellite System (GNSS) positioning techniques require the connection of base stations with rovers at measurement points during data acquisition. The methods used for the interaction and operation between base stations and rovers include real-time kinematic (RTK) measurements, static post-processing, and post-kinematic (PPK) solutions (Hofmann-Wellenhof et al., 2007). The real-time kinematic GNSS measurement method has demonstrated its effectiveness in surveying work (Tran Dinh Trong & Luong Ngoc Dung, 2024) and has been formalized in the current standards (Ministry of Natural Resources and Environment, 2015). Within the RTK framework, two primary subcategories exist: single-reference station RTK and network-based RTK. Despite the differences in approach (El-Mowafy, 2012), these methods share a common requirement: the operation of one or more reference stations, which can lead to unnecessary equipment costs.

The idea of conducting surveys without establishing reference stations has become feasible with the advent of precise point positioning (PPP) services (China Satellite Navigation Office, 2019a; European GNSS Supervisory Authority., 2023), which can be utilized with conventional receivers available to surveying engineers. Early analyses of the PPP-B2b service were conducted by Tang et al. (Tang et al., 2022), and the performance of the PPP-B2b solution was evaluated across mainland China and surrounding regions by Liu et al. (Y. Liu et al., 2022), in Vietnam by Tran et al (2023). As a result, GNSS receiver manufacturers have developed devices capable not only of receiving signals from multiple satellite navigation systems and supporting multi-frequency and multi-channel operations (ComNav Technology Ltd., 2020; Unicore Communications, 2022), but also of integrating free PPP features to attract customers and meet their precision needs. For instance, ComNav receivers offer such features (Comnav Tech, 2021). Additionally, an assessment of the long-term performance of Beidou PPP-B2b was conducted in 2022 by He et al. (He et al., 2023). The findings confirmed that the performance of the PPP-B2b product has shown significant improvements compared to the results reported two years ago. When combining Beidou Navigation Satellite System-3 (BDS-3) with Galileo, accuracy and convergence can improve by up to 50% compared to using a single system (Hou & Zhou, 2023). Although some risks have been identified by T. Liu et al (2017), the error sources have been analyzed, and their applications are becoming increasingly widespread (Elsheikh et al., 2023).

Two main drawbacks of PPP for surveying tasks are the extended initialization times compared to RTK positioning (15–30 minutes for PPP versus a few seconds for RTK) and the necessity to restart the entire process if the signal is lost. In terms of accuracy, (Naciri et al., 2023) demonstrated that integrating PPP with Galileo and GPS can achieve an accuracy of approximately 18.6 cm in both horizontal and vertical directions, with a convergence time of 7.5 minutes. More recently, Pintor et al. (Pintor et al., 2023) evaluated the High-Accuracy Service (HAS) for maritime operations, reporting accuracies of 0.22 m and 0.13 m at 95% and 68% confidence levels, respectively. These findings are consistent with the parameters outlined in the literature of the European GNSS Supervisory Authority (European GNSS Supervisory Authority., 2023). Additionally, Li and Pan (Li & Pan, 2021) conducted a study comparing the accuracy of this method across various analysis centers, finding that the combination of multiple systems can enhance both positioning accuracy and convergence time for post-processed kinematic PPP solutions.

The literature highlights a gap in evaluating the short-term precision positioning performance in localized areas with high demands for precise positioning, such as in civil engineering activities in Vietnam. While free PPP solutions are now available for certain receiver models currently offered in Vietnam, their adoption in surveying applications remains limited, despite their accuracy being well-documented in technical specifications. This study investigates the accuracy of free PPP solutions under open environmental conditions and compares their performance with that of a near-baseline RTK solution. The aims of the study will be addressed in the subsequent sections, including the PPP-B2b introduction, device, and experimental area; results and discussion; and conclusions.

2. PPP-B2b service, device and experiment area.

2.1. Beidou PPP-B2b service

Based on the announcement from the Chinese Satellite Navigation Office, the BDS-3 space constellation consists of 03 Geostationary Earth Orbit (GEO) satellites, 03 Inclined Geo-Synchronous Orbit (IGSO) satellites, and 24 Medium Earth Orbit (MEO) satellites at different altitudes (China Satellite Navigation Office, 2019b, 2019a). BDS-3 signals are transmitted on three frequencies: B1 (B1C-1575.42 MHz), B2 (B2a-1176.45 MHz, B2b-1207.14 MHz), and B3 (B3I-1268.52 MHz) (M. Lu. et al., 2019), with the signal on frequency B2b being utilised for PPP positioning methods and a range of other applications. The three GEO satellites broadcast orbit error correction parameters and satellite clock error corrections to users through the B2b frequency within China and neighbouring regions.

The PPP-B2b_I signal (S_{B2b_I})(t)) is generated by modulating the navigation message data (D_{B2b_I} (t)) and the range code (C_{B2b_I} (t)) (China Satellite Navigation Office, 2019a):

$$S_{B2b\_I}(t) = \frac{1}{\sqrt{2}}.D_{B2b\_I}(t).C_{B2b\_I}(t) \quad (1)$$

Where

$$D_{B2b\_I}(t) = \sum_{-\infty}^{\infty} d_{B2b\_I}[k]p_{B2b\_I}(t - kT_{B2b\_I}) \quad (2)$$

Where d_{B2b_I} is the navigation message data code, T_{B2b_I} is the chip width of the corresponding data code, and p_{B2b_I} is a rectangle pulse with a width of T_{B2b_I}.

The expression of range code C_{B2b_I} is as follows:

$$C_{B2b\_I}(t) = \sum_{n=-\infty}^{\infty} \sum_{k=0}^{N_{B2b\_I}-1} C_{B2b-I}[k]p_{T_{c\_B2b\_I}}(t - (N_{B2b\_I}n + k)T_{c\_B2b\_I}) \quad (3)$$

In Eq.3, C_{B2b_I} is a PPP-B2b_I ranging code sequence (possible values are ± 1), N_{B2b_I} is the ranging code length with a value of 10230, $T_{c\_B2b\_I}$= 1/$R_{c\_B2b\text{-}1}$ is the PPP-B2b_I chip period of ranging code, and $R_{c\_B2b\text{-}I}$ = 10.23 Mbps is the PPP = B2b_I chipping rate, and $p_{Tc\_B2b\_I}$ is a rectangle pulse with a duration of $T_{c\_B2b\_I}$.

In PPP, the pseudo-range and carrier phase observations can be written as follows (Tang et al., 2022):

$$P_i^S = \rho + cdt_r - cdt^S + I_i^S + T^S + c(b_{r,i} - b_i^S) + \varepsilon_P^S \quad (4)$$

$$\varphi_i^S = \rho + cdt_r - cdt^S - I_i^S + T^S + c(B_{r,i} - B_i^S) + \lambda_i N_i^S + \varepsilon_\varphi^S \quad (5)$$

Where: s,i refers to satellite and signal frequency, respectively
P,φ refers to pseudo-range observation and carrier phase observation
ρ denotes the distance from the satellite to the receiver
dt, dt^S refers to receiver errors and satellite clock errors
I_i^S refers to ionospheric delays
T^S refers to tropospheric delays
$b_{r,i}$,b_i^S refers to the pseudo-range code deviation of receivers and satellites
$B_{r,i}$,B_i^S refers to the hardware delay of receivers and satellites
N_i^S refers to the integer ambiguity of carrier phase observations
ε_P^S,ε_φ^S refers to the measurement noise of pseudo-range and carrier phase

2.1.1. Satellite orbit correction

As follows, the satellite position correction vector δX can be calculated via orbit corrections.

$$X_{orbit} = X_{broadcast} - \delta X \quad (6)$$

The satellite correction vector δX is as follows:

$$\delta X = [e_{radial} \quad e_{cross} \quad e_{along}].\delta O \quad (7)$$

Where: $e_{radial} = \frac{r}{|r|}$; ;

$e_{cross} = \frac{r \times \dot{r}}{|r \times \dot{r}|}$

and $e_{along} = e_{radial} \times e_{cross}$

In the formula, r, ṙ refers to the satellite position and velocity vector in the broadcast ephemeris, $e_{radial}, e_{along}, e_{cross}$ correspond to the unit vectors in the radial, tangential,and normal directions.

2.1.2. Satellite clock correction

Once the clock correction message successfully matches the broadcast ephemeris, the clock error $t_{broadcast}$ calculated from broadcast ephemeris can be corrected by a clock correction message C_0 as follows.

$$t_{satellite} = t_{broadcast} - \frac{C_0}{c} \quad (8)$$

Messages 2 and 4 describe satellite orbit and clock correction, as described in (China Satellite Navigation Office, 2019b).

The Beidou PPP-B2b signal's coverage includes the Asia-Pacific region, and BDS becomes the second GNSS system after the Galileo system to provide real-time PPP service (X. Lu et al., 2021).

2.2. Device and experiment procedure

To assess the performance of the PPP solution in an open and unobstructed environment, six points were chosen in an outdoor park area, free from obstructions or coverage by other features.

Figure 1. *Distribution of six measuring points and Base station position*

Six points (P1-P6) are distributed over an open area in the courtyard of an outdoor park with a rectangular shape as in Figure 2 and will be positioned using either RTK or PPP. For comparison, in addition to measuring PPP values at different times, we simultaneously conducted measurements using the single-base RTK method, with the base station located nearby (about 211 meters from the base to the rover, the consecutive distance between points Pi are smaller than 10 m). The rationale for selecting RTK as a basis for comparison includes two main reasons:

1. PPP and RTK functionalities are both available within a single GNSS receiver, allowing for a comparative evaluation based on each method's published specifications.
2. The RTK solution is widely recognised, validated, and established in current standards, making RTK measurement values a reliable reference for evaluating accuracy.

Both RTK and PPP methods use an N3 device, part of the ComNav-equipped K8 series, which supports the Precise Point Positioning (PPP) function, as illustrated in Figure 2. Table 1 provides its fundamental specifications.

To support users in measurement scenarios where the RTK solution is unstable or in locations without single-base station services or RTK networks, ComNav has developed the K8 firmware version that supports both PPP and RTK functionalities. Thus, when the RTK solution cannot be utilized, users can conveniently switch to the PPP mode with this firmware update. The results from the PPP solution are in real-time, leveraging the PPP algorithm integrated directly into the receiver's firmware. It is important to emphasize that this is a free feature providing real-time results, not post-processing on specialized high-accuracy software such as GAMIT, GLOCK, or other online PPP services.

Figure 2. N3 GNSS device with PPP function

Table 1. Basic specifications of N3 device

Specifications	Content
Channels	1198
RTK accuracy	8 mm + 1 ppm Horizontal 15 mm + 1 ppm Vertical
PPP accuracy	10 cm Horizontal Root Mean Square Error (H.RMS), 20 cm Vertical Root Mean Square Error (V.RMS)

The experiment consists of two sections and is conducted following these steps to evaluate the accuracy of the PPP solution.

Section 1 includes three steps

- **Step 1:** Measure the coordinates and elevations of six points (P1–P6) using the PPP solution at 5s -10s - 15s - 30s sample intervals for each point.
- **Step 2:** Invert the receiver until the signal is lost, then return it to an upright position and repeat the measurement procedure as conducted the second time.
- **Step 3:** Analyse and compare the coordinate values, elevations, and distances between points to those of six points (P1–P6) using the RTK method in single base-rover 4G working mode, with a short baseline distance of 211 meters between the base and the rover (5-second observation).

Section 2 is for the assessment of the convergence of PPP observations

- **Step 4:** Measuring at point P6 to evaluate the convergence of PPP observations.

To measure, the receiver is mounted on a vertical pole using a mini tripod with an alligator as shown in Figure 3.

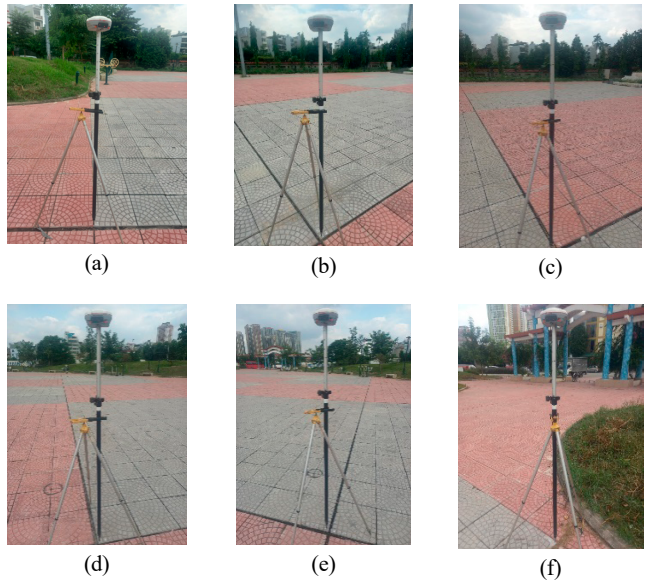

Figure 3. N3 receiver positioned at six points

Figures 3(a)-(f) show the instrument setup at measurement points P1 to P6. The points Pi are marked as crosses using correction pens. The vertical GNSS-RTK setup method was consistently applied to both PPP and RTK solutions based on a water bubble attached to the RTK pole. It should be noted that both methods use the same pole and centering accuracy has the same impact on the results. The reason for selecting values from the GNSS-RTK method for comparison is that, according to the technical specifications of the equipment, the accuracy of RTK is significantly higher than that of the free PPP method. Moreover, the distance from the base station to the RTK measurement points

is very close (211 m only). Regarding the coordinate system, both methods use the VN:2000 coordinate system, Transverse Mercator (TM) projection, and central meridian 105^0.

3. Results and discussion

In *steps 1 and 2* with the PPP solution, the fixed solution is achieved after around 32 minutes of connection. Coordinates and elevations of six points after four measuring times at 5s, 10s, 15s, and 30s in two rounds are in Table 3 (Appendix).

In step 3, with the RTK method, the fixed solution is achieved right after connecting to the base station due to the short distance. Their coordinates and elevations are in Table 4 (Appendix).

Regarding the PPP solution, the fixed solution is achieved 20 minutes after the receiver is inverted and the signal is lost (from 14:49 to 15:09). This duration is 12 minutes shorter than the first round. Examining the elevation column (Z column), it can be observed that the elevations from the PPP solution deviate significantly from those of the RTK solution. This discrepancy can be explained by the fact that RTK measurement points are connected to a single base station with elevations derived from national benchmarks. This means RTK measurement points have their elevations calculated within the national vertical reference system, whereas PPP measurement points do not.

According to the theory and published specifications, the coordinate values obtained from the RTK method have higher accuracy. By using the RTK-derived values as the true measurements, the deviations in the X, Y and Z directions for the six PPP measurement points across two observations at different times are calculated using the following formula:

$$\begin{aligned} \Delta X_{(PPP)i_t} &= X_{(PPP)i_t} - X_{(RTK)} \\ \Delta Y_{(PPP)i_t} &= Y_{(PPP)i_t} - Y_{(RTK)} \\ \Delta Z_{(PPP)i_t} &= Z_{(PPP)i_t} - Z_{(RTK)} \end{aligned} \tag{9}$$

The deviations of the six points between the two measurement times of the PPP method compared to the RTK method are shown in Figure 4 (a)-(m).

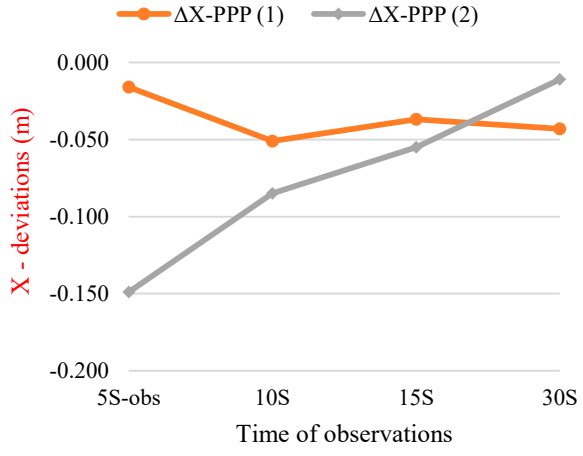

(a) X deviations of two rounds of PPP compared to the RTK method, point 1

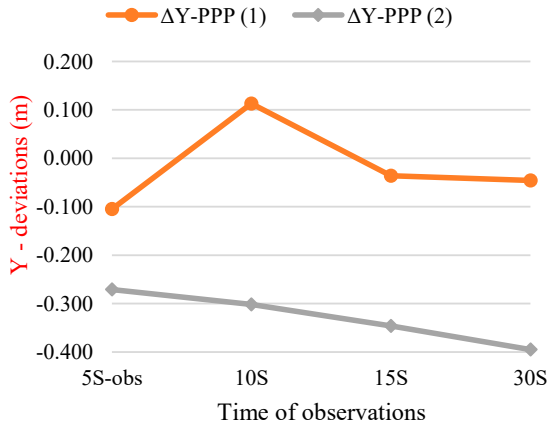

(b) Y deviations of two rounds of PPP compared to the RTK method, point 1

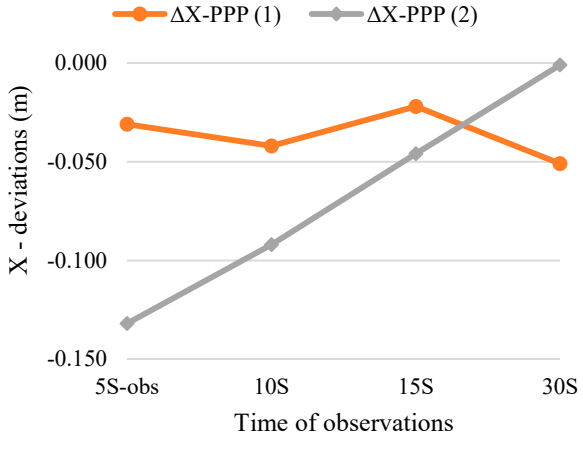

(c) X deviations of two rounds of PPP compared to the RTK method, point 2

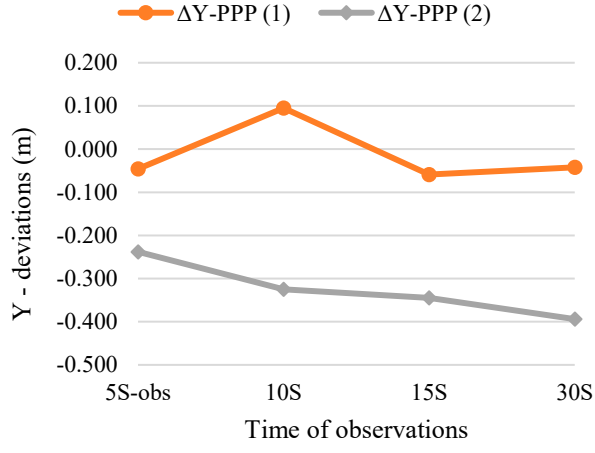

(d) Y deviations of two rounds of PPP compared to the RTK method, point 2

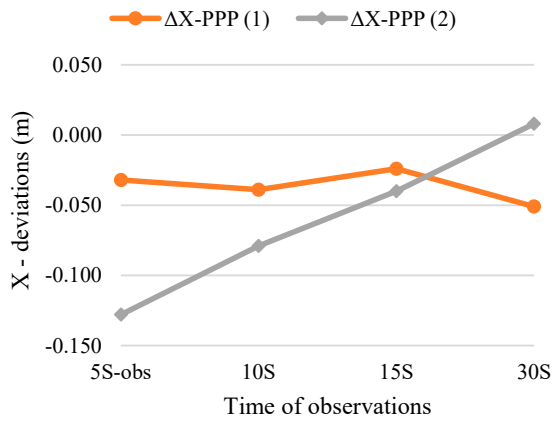

(e) X deviations of two rounds of PPP compared to the RTK method, point 3

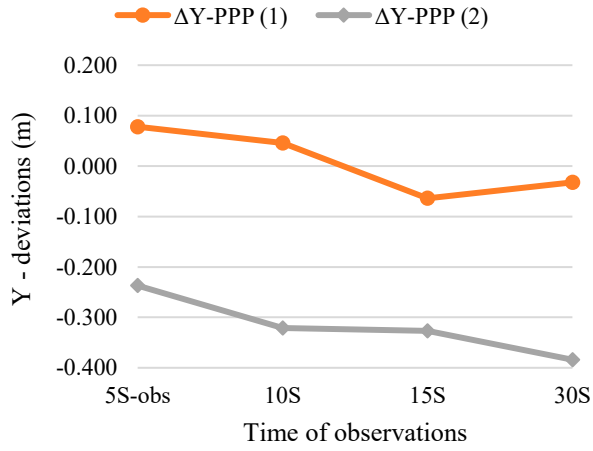

(f) Y deviations of two rounds of PPP compared to the RTK method, point 3

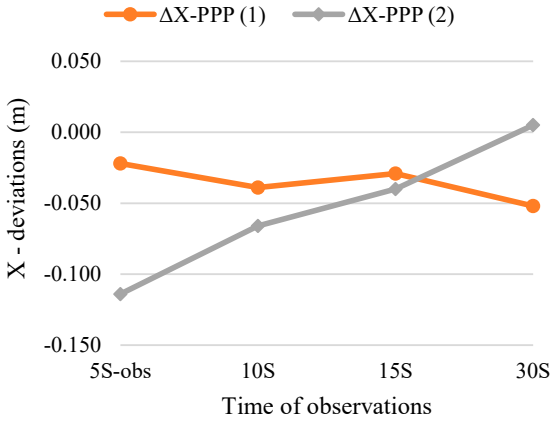

(g) X deviations of two rounds of PPP compared to the RTK method, point 4

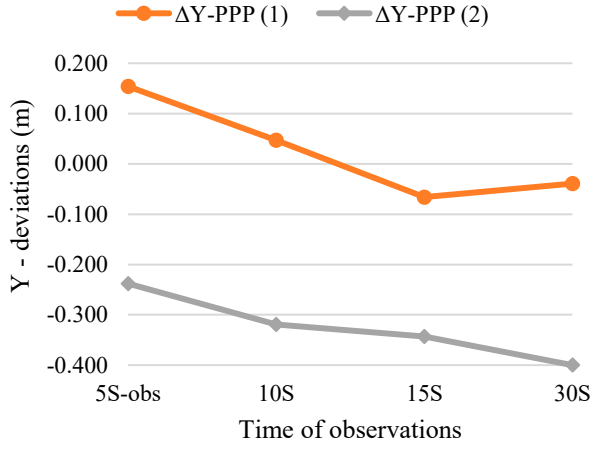

(h) Y deviations of two rounds of PPP compared to the RTK method, point 4

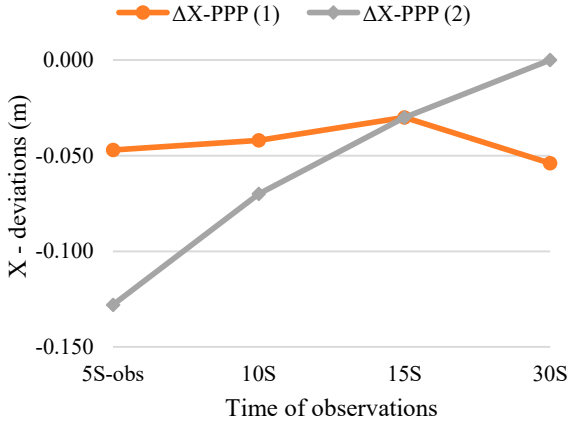

(i) X deviations of two rounds of PPP compared to the RTK method, point 5

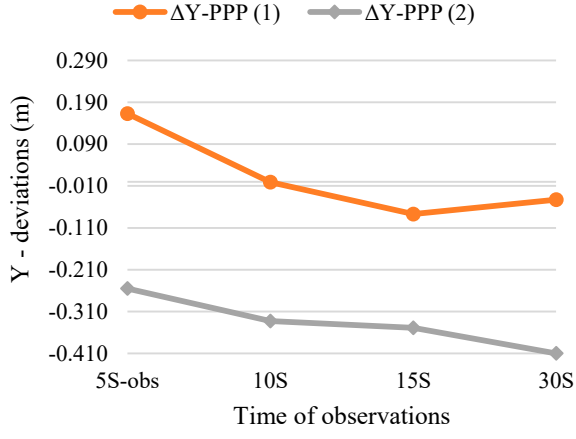

(k) Y deviations of two rounds of PPP compared to the RTK method, point 5

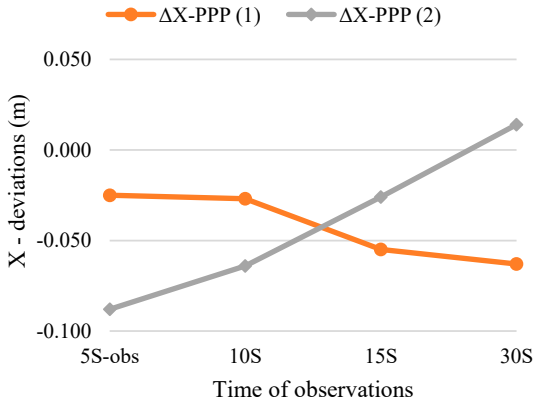

(l) X deviations of two rounds of PPP compared to the RTK method, point 6

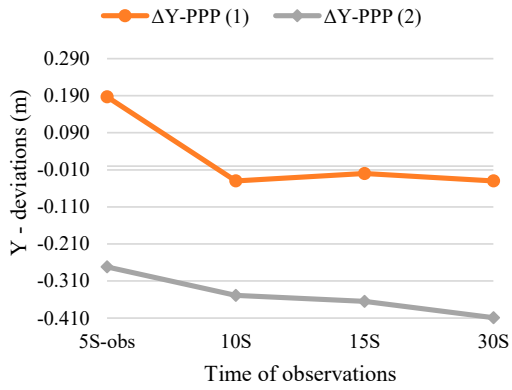

(m) Y deviations of two rounds of PPP compared to the RTK method, point 6

Figure 4. Oscillation of X, Y coordinates at 5-10-15-30s at six points

In Figure 4, the four points on the grey and orange lines correspond to the measurements taken at 5s, 10s, 15s, and 30s during two measurement sessions at points P1 to P6. The deviations in the X and Y coordinates of the six points during the first measurement session, with varying time intervals, range from 0.024 m to 0.038 m and from 0.142 m to 0.240 m, respectively. In the second measurement session, the deviations range from 0.102 m to 0.138 m for the X coordinate and from 0.124 m to 0.162 m for the Y coordinate, which are significantly larger compared to the first session.

When the X and Y coordinates are averaged over the measurements taken at 5s, 10s, 15s, and 30s, the deviation in the X coordinate of the six points ranges from -0.001 m to 0.038 m, and these deviations in the Y coordinate range from 0.310 m to 0.370 m.

The distances between the Pi points are relatively small, and the measurements were conducted within a short time frame; therefore, the points can be assumed to share similar environmental conditions. Taking the RTK-derived values as a reference, the RMSE of the X-coordinate at sampling intervals of 5s, 10s, 15s, and 30s across six points was calculated as 0.079 m, 0.054 m, 0.032 m, and 0.035 m, respectively. Similarly, for the Y-coordinate, the corresponding RMSE at the same sampling intervals were 0.183 m, 0.215 m, 0.226 m, and 0.259 m. A contrast is observed between the X and Y coordinate components. While the X component follows the expected theoretical trend-showing improved accuracy with increased sampling intervals (i.e., longer observation times) the Y component exhibits the opposite behaviour.

Considering the factors that may affect positioning accuracy such as satellite geometry, multipath errors, reference frame inconsistencies, and random noise the observed discrepancy is likely attributable to satellite geometry and random variations, given that the Pi points share the same location and favourable conditions for satellite signal reception. However, due to the limited number of samples in the experiment, it is difficult to draw a definitive conclusion regarding this phenomenon.

Regarding the elevation factors, Since the elevations obtained from the PPP and RTK methods are based on different vertical reference systems, we examine the variation in elevation between the two PPP measurements conducted at different observation times. Figure 5(a)-(f) shows the deviations in the Z factor of six points between the two measurement times.

The elevation deviations of the six points in the first measurement session range from 0.094 m to 0.229 m, while in the second session, they range from 0.028 m to 0.077 m. When averaging the elevation values across the measurements taken at 5s, 10s, 15s, and 30s, the deviations range from 0.267 m to 0.299 m. Figure 5 illustrates smaller variations in the height component across different sampling intervals during the second trial. This may be attributed to the receiver achieving a faster convergence and more stable performance in the second trial, compared to the first trial, which was conducted shortly after the receiver had been initialized for only 30 minutes.

Distance and different heights from point to point will be calculated and compared between the PPP and RTK methods. Distance deviations are shown in Figure 6(a)-(f).

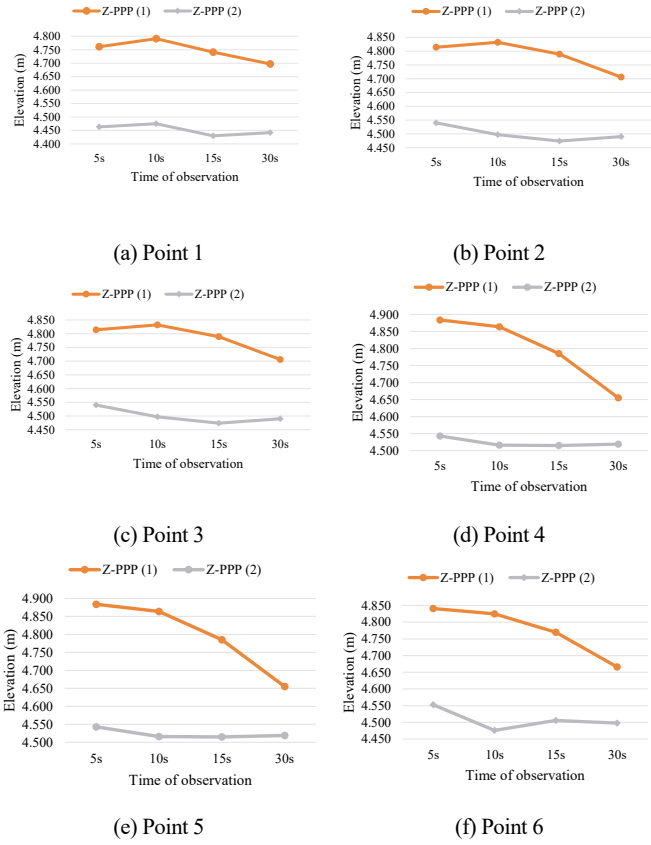

(a) Point 1 (b) Point 2

(c) Point 3 (d) Point 4

(e) Point 5 (f) Point 6

Figure 5. Oscillation of Z factor at 5-10-15-30s observations of two rounds of PPP

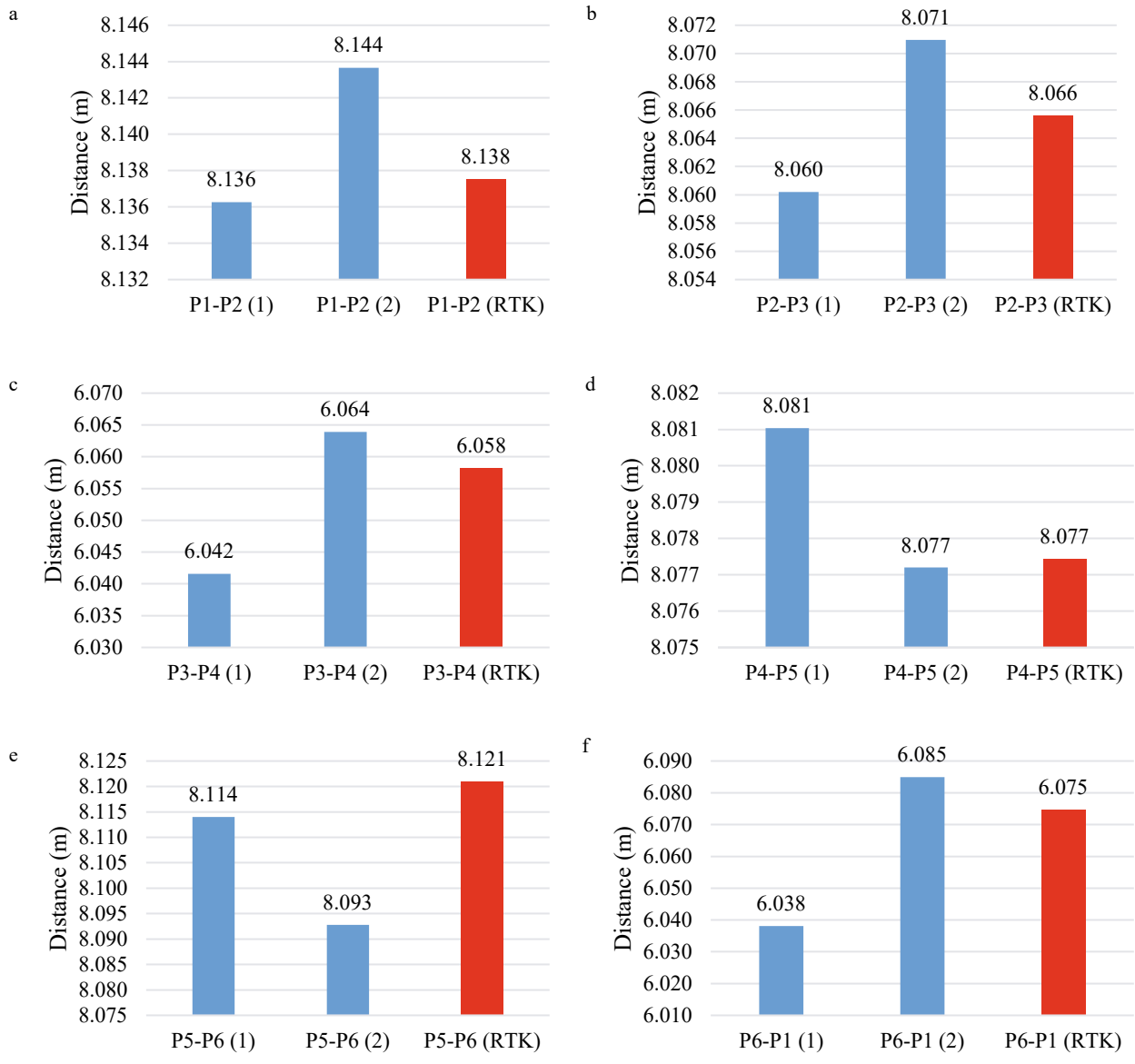

Figure 6. Distance comparison between PPP (two times) and RTK method

Although the deviations in the X and Y coordinates are relatively large between the two PPP measurement sessions, the deviations are negligible when calculating the distances between measurements and comparing them to distances obtained using the RTK method. The largest deviation in distance is observed between points P1 and P6 (0.047 m), while the deviations for all other distances are less than 0.030 m. It should be noted that the distances between points in each measurement session are calculated by averaging the distances from the measurements taken at 5s, 10s, 15s, and 30s. By applying a similar approach, let us examine the elevation differences between the points and their deviations. The results are presented in Figure 7(a)-(f).

It can be readily observed that the absolute elevation deviation between PPP and RTK is significant. This is understandable since RTK is corrected based on the national elevation reference point. However, using a similar approach as with distance measurements, the deviations in relative elevation differences are found to be very small, even smaller than those of the distance measurements. A more important observation is that, although the relative elevation differences between the points are small, they all have the same sign as those obtained using the RTK method.

Next, we examine the convergence of the PPP measurements at point P6, with a total of 156 measurements, each taken at 5-second intervals. The distribution chart of the X, Y, and Z parameters at point P6 is shown in Figure 8(a)-(c).

From Figure 8, some values in the Y coordinate and Z elevation series can be considered outliers. These outliers result in relatively large ranges of variation. The smallest range is observed in the X coordinate series, with a value of 0.042 m, while the range for the Y coordinate is 0.297 m, and the largest range is in the Z elevation, with a value of 0.657 m. It can be seen that the values considered outliers appear during the initial seconds of the measurement process at point P6.

It can be observed that, during the initial stages of the observation series, although the fixed solution was achieved after the manufacturer's recommended convergence time, the solution remained unstable. A similar trend to the first experiment is evident, in which the deviations in the Y and Z coordinate components were significantly larger than those in the X component. It is important to emphasize that this study utilizes objective results to evaluate the potential of the integrated PPP solution in standard GNSS receivers. For applications requiring high-precision positioning, outlier filtering algorithms, as employed in previous studies, should be considered (Ngoc Quang & Van Hien, 2022; Thi Nhung et al., 2021).

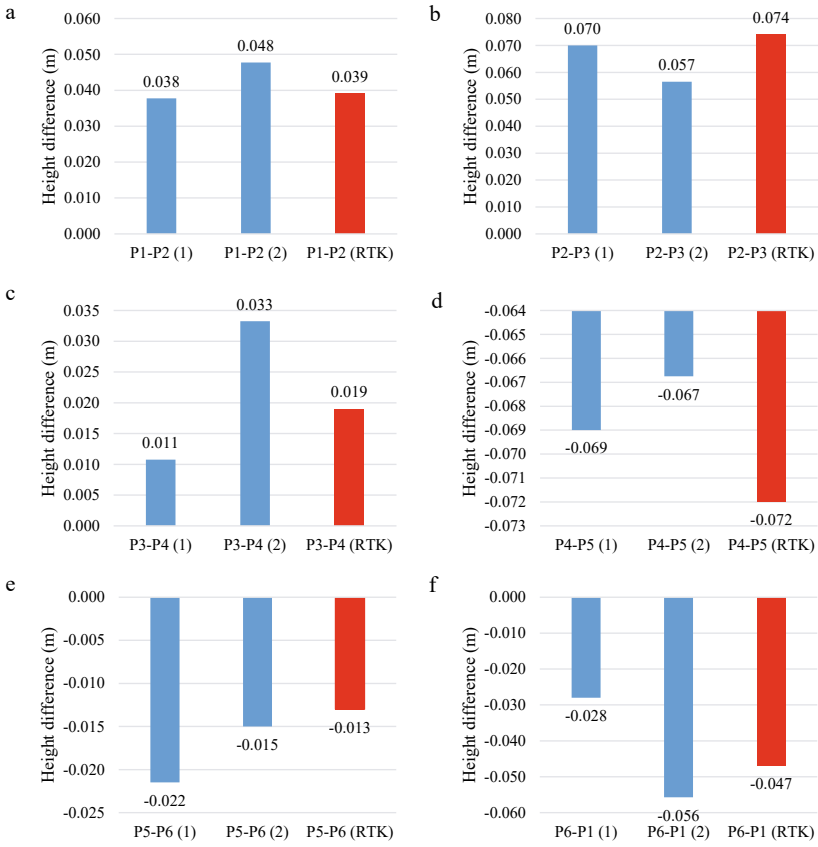

Figure 7. Height difference between PPP (two times) and RTK method

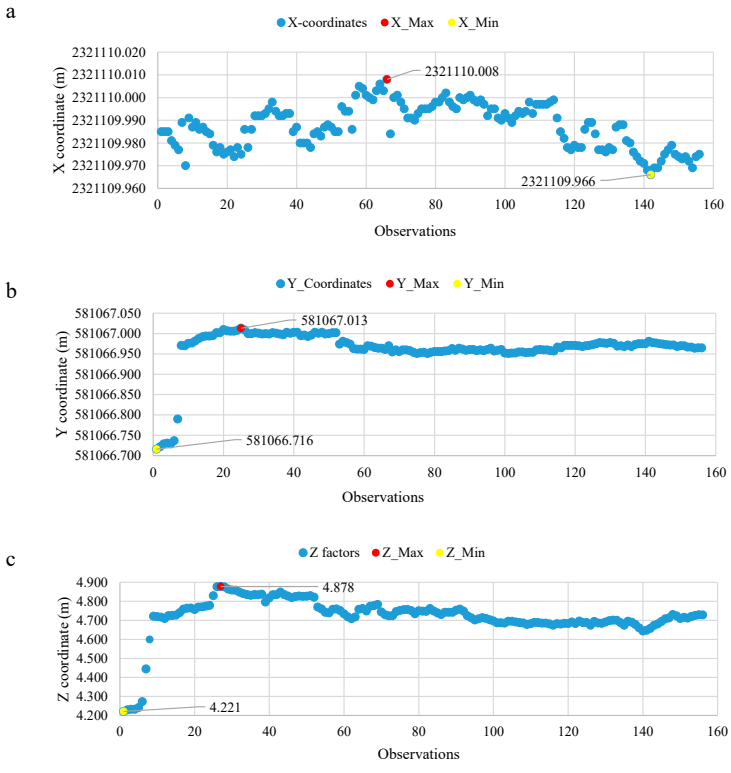

Figure 8. Distribution of horizontal factors and elevation at point P6

To examine the accuracy parameters of the data series, Table 2 provides basic descriptive statistics.

Table 2. Descriptive statistics of X, Y, and Z data

Parameters	X	Y	Z
Mean (m)	2321109.987	581066.964	4.719
Standard Error (m)	0.0008	0.0042	0.0091
Median (m)	2321109.988	581066.97	4.726
Mode (m)	2321109.985	581066.97	4.688
Standard Deviation (m)	0.0097	0.0526	0.1141
Sample Variance (m^2)	0.0001	0.0028	0.0130
Minimum (m)	2321109.966	581066.716	4.221
Maximum (m)	2321110.008	581067.013	4.878
Count	156	156	156
Confidence Level (95.0%) (m)	0.0015	0.0083	0.0180

Using the basic error evaluation formulas of Charles and Paul (2006), the standard deviation values for the X, Y, and Z coordinate series are 0.0097 m, 0.0526 m and 0.1141 m, respectively. Compared to the RTK method, the Z factor in the PPP method has the highest standard deviation, the same as the RTK solution.

4. Conclusion

Based on the experiment results, some outlines can be made as follows:

Firstly, the potential for conducting surveying tasks without the need for a base station, as required in the RTK method, can be partially realized with the free PPP solution. However, this is contingent upon the specific accuracy requirements of applications such as depth measurement, environmental pollution management, trajectory monitoring, and navigation. For more demanding applications, such as monitoring structural oscillations with large amplitude variations, advanced data processing solutions are essential.

Secondly, regarding accuracy, the free PPP solution available in the affordable and widely used N3 receiver produces results consistent with the specifications outlined in the device's datasheet (Comnav Tech, 2021). These results are also comparable to findings from previous studies (Naciri et al., 2023; Pintor et al., 2023)

Thirdly, further investigation is needed to assess the adoption of the free PPP solution under more detailed and varied scenarios, including specific objectives and measurement durations. This will facilitate a more comprehensive evaluation of the method's applicability. A notable issue identified in this study is the significant vertical deviation (approximately 2 meters) between the two methods, which is primarily attributed to inherent methodological differences. This study focuses on the application of free real-time PPP solutions. As a result, the positioning accuracy does not reach the level achievable with post-processed PPP methods used in prior studies, due to the absence of latency compensation. A notable discrepancy is observed in the height component, primarily due to the use of different vertical datums in the two approaches. To mitigate this, PPP observations can be referenced to a known benchmark within the local vertical system, allowing for height adjustment to align with RTK-derived values.

Finally, the results were obtained using a free PPP solution on a standard GNSS receiver operating in real-time, with both RTK and PPP capabilities. The findings support the integrated use of these two positioning methods in scenarios with limited 4G signal availability and in practical surveying applications such as forest area measurement, environmental monitoring, and damage assessment. This approach can serve as an alternative to handheld GPS devices, offering improved positioning accuracy while maintaining consistency in both coordinate and vertical reference systems.

Acknowledgments

The authors would like to acknowledge the financial support (No. B2024-MDA-08) from the Ministry of Education and Training of Vietnam.

References

Charles D, G., & Paul R, W. (2006). Adjustment Computations (Fourth Edi). John Wiley & Sons, INC, New Jersy, USA, 632pp.

China Satellite Navigation Office. (2019a). BeiDou Navigation Satellite System Signal In Space Interface Control Document Precise Point Positioning Service Signal PPP-B2b.

China Satellite Navigation Office. (2019b). Development of the BeiDou Navigation Satellite System (Version 4.0) (Issue December). http://en.beidou.gov.cn/SYSTEMS/Officialdocument/

Comnav Tech. (2021). N3_IMU_GNSS_Receiver, China.

ComNav Technology Ltd. (2020). K803 GNSS Module 30, China.

El-Mowafy, A. (2012). Precise Real-Time Positioning Using Network RTK. In Global Navigation Satellite Systems: Signal, Theory and Applications (Issue February 2012, pp. 161–187). InTech. https://doi.org/10.5772/29502

Elsheikh, M., Iqbal, U., Noureldin, A., & Korenberg, M. (2023). The Implementation of Precise Point Positioning (PPP): A Comprehensive Review. Sensors Review, 23, 1–25. https://doi.org/https://doi.org/10.3390/s23218874

European GNSS Supervisory Authority. (2023). Galileo High Accuracy Service : Service Definition Document (HAS SDD) (Issue 1).

He, Q., Chen, L., Liu, L., Zhao, D., Gong, X., Lou, Y., & Guan, Q. (2023). Long-Term Performance Evaluation of BeiDou PPP-B2b Products and Its Application in Time Service. Remote Sensing, 15(5), 1–16. https://doi.org/10.3390/rs15051358

Hofmann-Wellenhof, B., Lichtenegger, H., & Wasle, E. (2007). GNSS–global navigation satellite systems: GPS, GLONASS, Galileo, and more. Springer Science & Business Media, Austria, 546pp.

Hou, Z., & Zhou, F. (2023). Assessing the Performance of Precise Point Positioning (PPP) with the Fully Serviceable Multi-GNSS Constellations: GPS, BDS-3, and Galileo. Remote Sensing, 15(3). https://doi.org/10.3390/rs15030807

Li, X., & Pan, L. (2021). Precise point positioning with almost fully deployed bds-3, bds-2, gps, glonass, galileo and qzss using precise products from different analysis centers. In Remote Sensing (Vol. 13, Issue 19). https://doi.org/10.3390/rs13193905

Liu, T., Yuan, Y., Zhang, B., Wang, N., Tan, B., & Chen, Y. (2017). Evaluation of the Integrity Risk for Precise Point Positioning. Journal of Geodesy, 91(3), 253–268. https://doi.org/10.1007/s00190-016-0960-3

Liu, Y., Yang, C., & Zhang, M. (2022). Comprehensive Analyses of PPP- B2b Performance in China and Surrounding Areas. Remote Sensing, 14(3), 1–28. https://doi.org/10.3390/rs14030643

Lu., M., Li., W., Yao, Z., Cui, X., & Department. (2019). Overview of BDS III new signals. Navigation, 19–35. https://doi.org/10.1002/navi.296

Lu, X., Chen, L., Shen, N., Wang, L., Jiao, Z., & Chen, R. (2021). Decoding PPP Corrections from BDS B2b Signals Using a Software- defined Receiver- an Initial Performance Evaluation. IEEE Sensors Journal, 21(6), 7871–7883. https://doi.org/10.1109/JSEN.2020.3041486

Ministry of Natural Resources and Environment. (2015). Circular No. 68/2015/TT-BTNMT of the Ministry of Natural Resources and Environment: Technical regulations for direct terrain measurement to serve the establishment of topographic maps and geographic database at 1:500 scale, 1:1000, 1:2000, 1:5000, Vietnam.

Naciri, N., Yi, D., Bisnath, S., de Blas, F. J., & Capua, R. (2023). Assessment of Galileo High Accuracy Service (HAS) test signals and preliminary positioning performance. GPS Solutions, 27(2). https://doi.org/10.1007/s10291-023-01410-y

Ngoc Quang, V., & Van Hien, L. (2022). Filtering Outliers in GNSS Time Series Data in Real-Time Bridge Monitoring. Proceedings of the 4th International Conference on Sustainability in Civil Engineering, 657–663. https://doi.org/10.1007/978-981-99-2345-8

Pintor, P., Lopez-Martinez, M., Gonzalez, E., Safar, J., & Boyle, R. (2023). Testing Galileo High-Accuracy Service (HAS) in Marine Operations. Journal of Marine Science and Engineering, 11(2375), 1–13. https://doi.org/10.3390/jmse11122375

Tang, J., Lyu, D., Zeng, F., Ge, Y., & Zhang, R. (2022). Comprehensive Analysis of PPP-B2b Service and Its Impact on BDS-3/GPS Real-Time PPP Time Transfer. Remote Sensing, 14(21), 1–22. https://doi.org/10.3390/rs14215366

Thi Nhung, L., Männel, B., Jarema, M., Seemala, G. K., Heki, K., & Schuh, H. (2021). Selection of an optimal algorithm for outlier detection in GNSS time series. EGU General Assembly 2021. https://doi.org/10.5194/egusphere-egu21-1598

Tran, D. T., Nguyen, D. H., Vu, N. Q., & Nguyen, Q. L. (2023). Crustal displacement in Vietnam using CORS data during 2018-2021. Earth Sciences Research Journal, 27(1), 27–36. https://doi.org/10.15446/esrj.v27n1.102630

Tran Dinh Trong, & Luong Ngoc Dung. (2024). Study on the positioning efficiency of GNSS RTK for road profile surveys - case study in Vietnam. Journal of Science and Technology in Civil Engineering (JSTCE) - HUCE, 18(2), 86–98. https://doi.org/10.31814/stce.huce2024-18(2)-07

Unicore Communications. (2022). UM982 GPS/BDS/GLONASS/Galileo/QZSS All-constellation Multi-frequency High Precision Positioning & Heading Module. China.

Appendix

Table 3. Coordinates and elevations of six points (PPP method) at different times

Time	Point	Sample interval	N (m)	E (m)	Z (m)	Measurement Round
10/30/2023 14:12	P1	5s	2321111.835	581072.692	4.761	Round 1
10/30/2023 14:14	P2		2321119.621	581070.435	4.814	
10/30/2023 14:16	P3		2321127.354	581068.270	4.914	
10/30/2023 14:18	P4		2321125.658	581062.533	4.951	
10/30/2023 14:19	P5		2321117.895	581064.859	4.884	
10/30/2023 14:21	P6		2321110.129	581067.151	4.841	
10/30/2023 14:25	P1	10s	2321111.800	581072.910	4.791	
10/30/2023 14:27	P2		2321119.610	581070.576	4.832	
10/30/2023 14:29	P3		2321127.347	581068.238	4.900	
10/30/2023 14:30	P4		2321125.641	581062.426	4.925	
10/30/2023 14:31	P5		2321117.900	581064.695	4.864	
10/30/2023 14:32	P6		2321110.127	581066.924	4.825	
10/30/2023 14:33	P1	15s	2321111.814	581072.761	4.741	
10/30/2023 14:34	P2		2321119.630	581070.422	4.789	
10/30/2023 14:35	P3		2321127.362	581068.128	4.854	
10/30/2023 14:36	P4		2321125.651	581062.313	4.852	
10/30/2023 14:37	P5		2321117.912	581064.619	4.785	
10/30/2023 14:38	P6		2321110.099	581066.944	4.770	
10/30/2023 14:39	P1	30s	2321111.808	581072.751	4.697	
10/30/2023 14:41	P2		2321119.601	581070.439	4.706	
10/30/2023 14:43	P3		2321127.335	581068.160	4.753	
10/30/2023 14:45	P4		2321125.628	581062.340	4.736	
10/30/2023 14:46	P5		2321117.888	581064.653	4.655	
10/30/2023 14:49	P6		2321110.091	581066.924	4.666	

Time	Point	Sample interval	N (m)	E (m)	Z (m)	Measurement Round
10/30/2023 15:09	P1	5s	2321111.702	581072.526	4.463	Round 2 (after up and down N3 receiver)
10/30/2023 15:10	P2		2321119.520	581070.243	4.540	
10/30/2023 15:11	P3		2321127.258	581067.955	4.581	
10/30/2023 15:12	P4		2321125.566	581062.141	4.625	
10/30/2023 15:13	P5		2321117.814	581064.441	4.543	
10/30/2023 15:14	P6		2321110.066	581066.692	4.553	
10/30/2023 15:16	P1	10s	2321111.766	581072.495	4.475	
10/30/2023 15:17	P2		2321119.560	581070.156	4.497	
10/30/2023 15:18	P3		2321127.307	581067.871	4.540	
10/30/2023 15:19	P4		2321125.614	581062.060	4.575	
10/30/2023 15:20	P5		2321117.872	581064.363	4.516	
10/30/2023 15:21	P6		2321110.090	581066.615	4.476	
10/30/2023 15:22	P1	15s	2321111.796	581072.451	4.430	
10/30/2023 15:23	P2		2321119.606	581070.136	4.474	
10/30/2023 15:24	P3		2321127.346	581067.865	4.551	
10/30/2023 15:25	P4		2321125.640	581062.036	4.584	
10/30/2023 15:26	P5		2321117.912	581064.347	4.515	
10/30/2023 15:27	P6		2321110.128	581066.599	4.506	
10/30/2023 15:28	P1	30s	2321111.840	581072.402	4.442	
10/30/2023 15:30	P2		2321119.651	581070.087	4.490	
10/30/2023 15:31	P3		2321127.394	581067.808	4.555	
10/30/2023 15:33	P4		2321125.685	581061.979	4.576	
10/30/2023 15:34	P5		2321117.942	581064.286	4.519	
10/30/2023 15:35	P6		2321110.168	581066.555	4.498	

Table 4. Coordinates and elevations of six points (RTK method)

Time	Point	N (m)	E (m)	Z (m)
2023Y10M30D15H47M55S	P1	2321111.8510	581072.7970	6.2750
2023Y10M30D15H48M59S	P2	2321119.6520	581070.4810	6.3140
2023Y10M30D15H49M49S	P3	2321127.3860	581068.1920	6.3880
2023Y10M30D15H50M32S	P4	2321125.6800	581062.3790	6.4070
2023Y10M30D15H51M40S	P5	2321117.9420	581064.6960	6.3350
2023Y10M30D15H52M39S	P6	2321110.1540	581066.9640	6.3220